Letter

Transport barriers to self-propelled particles in fluid flows

Simon A. Berman [1,*] John Buggeln,[2] David A. Brantley [1,3]
Kevin A. Mitchell [1,†] and Thomas H. Solomon [2,‡]
[1]*Department of Physics, University of California, Merced, California 95344, USA*
[2]*Department of Physics and Astronomy, Bucknell University, Lewisburg, Pennsylvania 17837, USA*
[3]*Lawrence Livermore National Laboratory, Livermore, California 94550, USA*

(Received 7 August 2020; accepted 24 December 2020; published 14 January 2021)

We present theory and experiments demonstrating the existence of invariant manifolds that impede the motion of microswimmers in two-dimensional fluid flows. One-way barriers are apparent in a hyperbolic fluid flow that block the swimming of both smooth-swimming and run-and-tumble *Bacillus subtilis* bacteria. We identify key phase-space structures, called swimming invariant manifolds (SwIMs), that serve as separatrices between different regions of long-time swimmer behavior. When projected into xy space, the edges of the SwIMs act as one-way barriers, consistent with the experiments.

DOI: 10.1103/PhysRevFluids.6.L012501

Dynamically defined transport barriers [1,2] impede the motion of passive particles in a wide range of fluids, from microbiological and microfluidic flows to oceanic, atmospheric, and stellar flows. For steady and time-periodic flows, transport barriers are identified with invariant manifolds of fixed points and Kolmogorov-Arnold-Moser surfaces [3–5]. More recently, these ideas have been extended to aperiodic and turbulent flows [6–10]. However, in many systems of fundamental and practical importance, the tracers are *active* rather than passive. Examples include propagating chemical reaction fronts [11,12], aquatic vessels [13], and artificial and biological microswimmers [14,15], including Janus particles [16,17] and flagellated bacteria [18,19].

Invariant manifold theory has previously been extended to incorporate propagating reaction fronts in a flow [20–24]. This theory identifies analogs of passive transport barriers, called *burning invariant manifolds* (BIMs), which are one-way barriers to front propagation. Experiments on front propagation in driven fluid flows [25–28] demonstrate the physical significance of these theories. Despite this success with reaction fronts, a comparable understanding of more general active systems is lacking.

This paper presents theory and supporting experiments for a foundational and universal invariant manifold framework that describes barriers for active tracers in laminar fluid flows. We focus on self-propelled particles, i.e., swimmers, and propose the existence of *swimming invariant manifolds* (SwIMs) that (i) act as absolute barriers blocking the motion of smooth swimmers in position-orientation space; (ii) project to one-way barriers in position space; and (iii) provide insight into the motion of nonsmooth (e.g., tumbling) swimmers. We also find that (iv) one-way barriers exist even for tumbling swimmers, and these barriers turn out to be identical to the BIMs that were previously shown to be barriers for reaction fronts [20]. Our experiments use smooth-swimming and run-and-tumble strains of *Bacillus subtilis* bacteria [Fig. 1(a), inset] as active tracers in a laminar,

*sberman4@ucmerced.edu
†kmitchell@ucmerced.edu
‡tsolomon@bucknell.edu

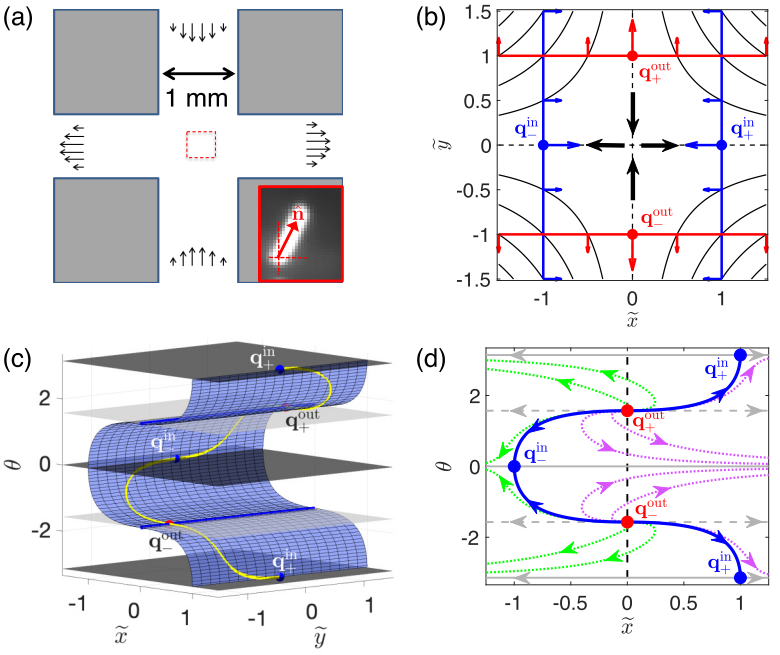

FIG. 1. (a) Cross-flow experiment; data obtained are in the red square. Inset: 100× image of a fluorescent *B. subtilis*. (b) SFPs and SwIM edges (in red and blue) of the hyperbolic flow; $\alpha > 0$. Arrows indicate the direction of $\hat{\mathbf{n}}$ (and the blocking direction) for the equilibria and the SwIM edges. Streamlines of the flow are plotted in black. (c) Stable SwIMs (blue surfaces) of the $\mathbf{q}_\pm^{\rm in}$ SFPs for $\alpha = 1$. Black (gray) planes show stable (unstable) invariant surfaces. Yellow curves represent heteroclinic orbits connecting pairs of SFPs. (d) Constant-y cross section of the swimmer phase space. Blue orbits represent cross sections of the stable SwIMs.

hyperbolic flow in a microfluidic cross-channel [Fig. 1(a)]. Absent Brownian motion, passive tracers in a linear hyperbolic flow cannot traverse the passive invariant manifolds (separatrices) forming a cross along the channel centerlines [dashed lines in Fig. 1(b)], whereas self-propelled tracers can. Nevertheless, we show that barriers to active particles still exist. We also present theory extending our analysis to the mixing of swimmers in a vortex flow.

In our model, an ellipsoidal swimmer in two dimensions is described by $\mathbf{q} = (\mathbf{r}, \hat{\mathbf{n}})$, comprising its position $\mathbf{r} = (x, y)$ and swimming direction $\hat{\mathbf{n}} = (\cos\theta, \sin\theta)$. Absent noise and active torques, a swimmer with a fixed swimming speed v_0 in a fluid velocity field $\mathbf{u}(\mathbf{r})$ obeys [14,15,29,30]

$$\dot{\mathbf{r}} = \mathbf{u} + v_0\hat{\mathbf{n}}, \quad \dot{\theta} = \frac{\omega_z}{2} + \alpha\,\hat{\mathbf{n}}_\perp \cdot \mathbf{E} \cdot \hat{\mathbf{n}}, \tag{1}$$

where $\omega_z = \hat{\mathbf{z}} \cdot (\nabla \times \mathbf{u})$ is the vorticity, $\hat{\mathbf{n}}_\perp = (-\sin\theta, \cos\theta)$, and $\mathbf{E} = (\nabla\mathbf{u} + \nabla\mathbf{u}^{\rm T})/2$ is the symmetric rate-of-strain tensor. The shape parameter α equals $(\gamma^2 - 1)/(\gamma^2 + 1)$, where γ is the aspect ratio of the ellipse; α varies from -1 to 1, where $\alpha = 0$ is a circle, and $|\alpha| = 1$ is a rod. Positive (negative) values of α correspond to swimming parallel (perpendicular) to the major axis. The case $\alpha = -1$ coincides with the dynamics of a propagating front element [20] and the optimal (least-time) swimmer trajectories [13,31].

Equation (1) with $v_0 = 0$ models passive transport. The linear hyperbolic flow, $\mathbf{u} = (Ax, -Ay)$ has a passive saddle fixed point at $\mathbf{r} = \mathbf{0}$. The y and x axes are the stable and unstable manifolds, respectively, defined as invariant sets whose points approach the passive fixed point forwards and backwards in time. Passive particles cannot cross these passive manifolds [Fig. 1(b)].

For swimmers in the hyperbolic flow, Eq. (1) becomes

$$\dot{\widetilde{x}} = \widetilde{x} + \cos\theta, \quad \dot{\widetilde{y}} = -\widetilde{y} + \sin\theta, \quad \dot{\theta} = -\alpha \sin(2\theta), \tag{2}$$

with dimensionless variables $\widetilde{\mathbf{r}} = (A/v_0)\mathbf{r}$ and $\widetilde{t} = At$. The natural analogs of the passive fixed point are the fixed points of Eq. (2), called *swimming fixed points* (SFPs) [32]. There are four SFPs. Two SFPs lie on the y axis with the swimmer facing outward: $\mathbf{q}_{\pm}^{\text{out}} = (\pm\hat{\mathbf{y}}, \pm\hat{\mathbf{y}})$. The remaining SFPs lie on the x axis with the swimmer facing inward: $\mathbf{q}_{\pm}^{\text{in}} = (\pm\hat{\mathbf{x}}, \mp\hat{\mathbf{x}})$. The SFPs are plotted in Figs. 1(b)–1(d). These equilibria are saddles, for all v_0 and α.

We set $\alpha = 1$, approximating the shape of *B. subtilis* as a rod. Since the SFPs are saddles, they possess stable and unstable manifolds in the $\widetilde{x}\widetilde{y}\theta$ phase space, which we call swimming invariant manifolds, or SwIMs, to distinguish them from those for passive advection. For $\alpha > 0$, the inward SFPs have two stable and one unstable directions. Hence, they each possess a two-dimensional (2D) stable SwIM [Fig. 1(c)], which together form a warped sheet in phase space, referred to simply as *the* SwIM. The SwIM separates phase space into two regions: to the left [right] of the SwIM, all swimmer trajectories are ultimately leftward-escaping (LE) [rightward-escaping (RE)] [Fig. 1(d)].

The SwIM is only a strict phase-space barrier for *perfectly* smooth-swimming tracers, which is not the case for real swimmers. For example, tumbling bacteria apply brief active torques to suddenly change their swimming direction; we expect these bacteria to be able to cross the SwIM during their tumbles. Even for "smooth-swimming" bacteria, the swimming direction fluctuates; bacteria wiggle as they swim due to rotational diffusion [33,34] and the kinematics of swimming with helical flagella [35]. Hence, bacteria near the SwIM may occasionally cross it due to these small fluctuations in θ.

The SwIM shown in Fig. 1(c) produces *one-way* barriers to swimmers when projected onto the $\widetilde{x}\widetilde{y}$ plane, barriers that are valid even for noisy swimmers. For a general 2D flow $\mathbf{u}(\mathbf{r})$, a static, parametrized curve $\mathbf{R}(s)$ with local normal vector $\hat{\mathbf{N}}(s)$ is a one-way barrier to swimmers when the swimmer velocity across the curve, $[\mathbf{u}(\mathbf{R}(s)) + v_0\hat{\mathbf{n}}] \cdot \hat{\mathbf{N}}(s)$, is nonpositive for all $\hat{\mathbf{n}}$. Hence, if the condition

$$-\frac{\mathbf{u}(\mathbf{R}(s)) \cdot \hat{\mathbf{N}}(s)}{v_0} \geqslant 1, \quad \text{for all } s, \tag{3}$$

is met, then the curve $\mathbf{R}(s)$ is a one-way barrier with local blocking direction $\hat{\mathbf{N}}(s)$. For the hyperbolic flow, all nonstationary trajectories along the line $\widetilde{x} = -1$ move leftward, regardless of θ [Fig. 1(d)]. Evaluating the left-hand side of Eq. (3) along this line [in dimensional variables, $\mathbf{R}(s) = (-v_0/A, s)$ and $\hat{\mathbf{N}} = \hat{\mathbf{x}}$], we obtain identically 1. Therefore, this line is a one-way barrier, preventing rightward motion but not leftward. Furthermore, because Eq. (3) is independent of α and the time dependence of $\hat{\mathbf{n}}$, we expect any curve satisfying it to be a one-way barrier for all swimmers, *regardless of their shape or motility pattern*. In particular, we expect the line $\widetilde{x} = -1$ to be a barrier to both the smooth-swimming and the tumbling strains of bacteria.

Geometrically, Figs. 1(c) and 1(d) show that the line $\widetilde{x} = -1$ is the leftmost extent of the 2D SwIM projected onto the $\widetilde{x}\widetilde{y}$ plane, i.e., it is the left edge of the SwIM. By symmetry, the right SwIM edge $\widetilde{x} = 1$ is also a one-way barrier, which allows swimmers to pass through it from left to right, but not vice versa. Hence, the stable SwIM edges form barriers to inward-swimming particles. Similarly, the horizontal edges of the 2D unstable SwIMs of the outward SFPs form one-way barriers, blocking outward-swimming particles [Fig. 1(b)].

We test our theoretical predictions with microfluidic experiments on swimming bacteria. We fabricate polydimethylsiloxane (PDMS) cells with channels of width and depth 1 mm in a cross-shaped geometry [Fig. 1(a)]. Dilute bacterial suspensions are pumped into both ends of the vertical channel and out both ends of the horizontal channel using syringe pumps. Microscopy movies are recorded in the center of the channel at 40×. Passive tracer analysis reveals that the flow in the center [red square in Fig. 1(a)] is well approximated by a planar, 2D linear hyperbolic flow. The bacteria used are *B. subtilis*, either the smooth-swimming strain OI4139 or the

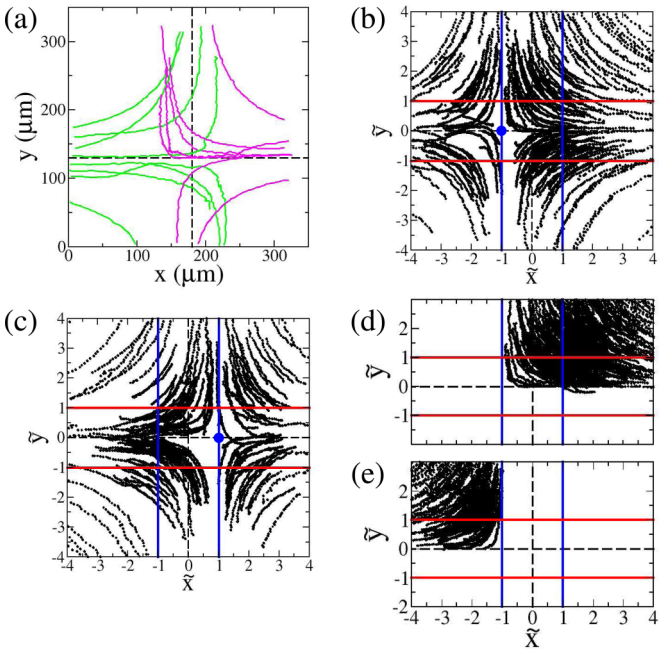

FIG. 2. (a) Experimental trajectories for smooth-swimming *B. subtilis*; $A = 0.44\ \mathrm{s}^{-1}$. Passive manifolds are shown by dashed lines. (b) Right-swimming trajectories. Positions are scaled by v_0/A. The theoretically predicted SFP $\mathbf{q}_-^{\mathrm{in}}$ (blue circle) and the SwIM edges (red and blue lines) are shown. (c) Left-swimming trajectories and $\mathbf{q}_+^{\mathrm{in}}$. (d) Rectified plot showing all trajectories as if leaving through the upper-right quadrant. (e) All trajectories entering with $|\widetilde{x}| > 1$ rectified to enter the upper-left quadrant.

green-fluorescent-protein-expressing (GFP) run-and-tumble strain 1A1266. The bacteria's swimming speeds v_0 in the flow have a mean of 25 and 16 μm/s and a standard deviation of 11 and 6 μm/s for the smooth-swimming and tumbling GFP strains, respectively. Though the bacteria swim in three dimensions, we obtain trajectories only for those whose motion is predominantly 2D (according to the protocol described in the Supplemental Material, Sec. 1.2 [36]), corresponding well to the 2D theory.

Figure 2 shows trajectories of smooth-swimming bacteria, some of which overlap [Fig. 2(a)]. Trajectories of *passive*, nonswimming bacteria in the same experiment (Supplemental Material, Fig. S1 [36]) are blocked by the vertical passive separatrix [dashed line in Fig. 2(a)]. Hence, the region in Fig. 2(a) where the LE and RE swimmer trajectories overlap is a signature of the self-propulsion of the swimmers. Our theory predicts that the width of this region is the distance between the vertical SwIM edges shown in Fig. 1(b), i.e., $2v_0/A$. In the experiments, v_0 is approximately constant in time for individual bacteria; however, different bacteria have different values for v_0 [37]. Consequently, the width of the overlap region is undetermined in Fig. 2(a).

Variations in v_0 are accounted for by rescaling the spatial coordinates by v_0/A, as in Eq. (2). The scaled, nondimensional trajectories are shown in Figs. 2(b)–2(e). The location of the inward SFPs and their SwIM edges is revealed by plotting trajectories for right-swimming and left-swimming bacteria separately [Figs. 2(b) and 2(c)]. The behavior of inward-swimming bacteria near an inward SFP is similar to that of a passive tracer moving near the hyperbolic fixed point. The key difference is that active tracers moving near SFPs can cross the SwIM edge from $|\widetilde{x}| < 1$ to $|\widetilde{x}| > 1$ but not in the other direction.

The experimental data are consistent with the theoretically predicted one-way barrier property of the SwIM edges. This is clearest when we use the symmetry of Eqs. (2) [$(\widetilde{y}, \theta) \mapsto (-\widetilde{y}, -\theta)$ and $(\widetilde{x}, \theta) \mapsto (-\widetilde{x}, \pi - \theta)$] to rectify the trajectories, such that all trajectories are displayed as though

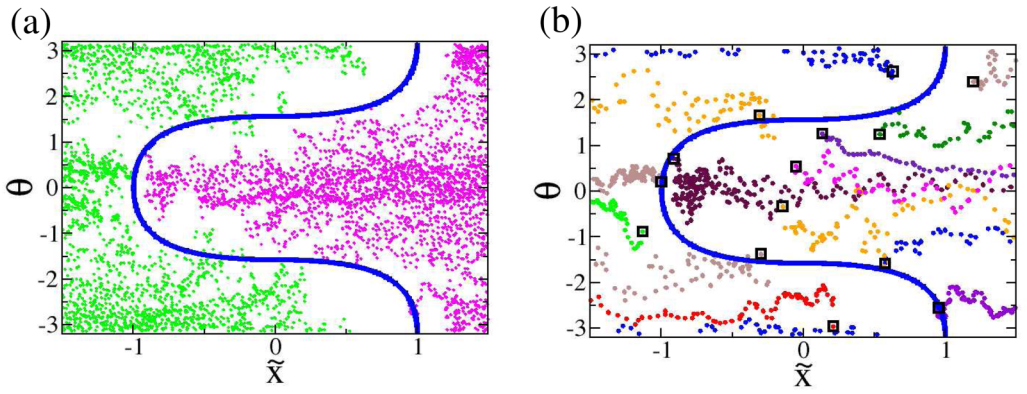

FIG. 3. Experimental $\tilde{x}\theta$ trajectories for smooth-swimming *B. subtilis*; $A = 0.44\ \mathrm{s}^{-1}$. The theoretical SwIM ($\alpha = 1$) is plotted in blue. (a) All trajectories. Leftward-escaping trajectories are shown in green, and rightward-escaping trajectories in magenta. (b) Selected trajectories; the beginning of each is marked with an open square.

entering from the upper inlet and escaping to the right. Under this transformation, Fig. 2(d) shows that all trajectories are bounded from the left by the SwIM edge at $\tilde{x} = -1$, in agreement with the theory. Indeed, any bacterium crossing this SwIM edge from left to right would violate the one-way barrier property. Furthermore, all bacteria that enter with $|\tilde{x}| > 1$ [Fig. 2(e), rectified such that initial $\tilde{x} < -1$] are swept away from the center of the cell, consistent with the SwIM edges at $|\tilde{x}| = 1$ as barriers to inward-swimming bacteria. Note that a single experiment with a fixed value of A inherently probes a range of values of the key parameter v_0/A, owing to the natural heterogeneity of bacterial swimming speeds. The data from an experiment in a slower flow are also consistent with our theoretical predictions (Supplemental Material, Fig. S2 [36]).

The delineation between LE and RE swimmers by the SwIM in the $\tilde{x}\theta$ plane is shown experimentally in Fig. 3 (see [36] for the measurement of θ). Most of the trajectories in Fig. 3(a) respect this barrier, although there is a slight breach of the SwIM for some of the bacteria, due to the variations in θ discussed previously. These vertical fluctuations in individual trajectories [Fig. 3(b)] cause momentary crossings of the "horizontal" part of the SwIM.

Angular fluctuations are, of course, particularly pronounced for the tumbling strain of bacteria [Fig. 4(a)], leading to highly irregular $\tilde{x}\theta$ trajectories. However, for bacteria with well-defined tumble events, the $\tilde{x}\theta$ trajectories [Fig. 4(b)] give insight into the short-term direction (right or left) of their $\tilde{x}\tilde{y}$ motion [Fig. 4(c)]. The bacterium in these two plots begins to the right of the SwIM; the corresponding $\tilde{x}\tilde{y}$ trajectory moves to the right during this period. The bacterium undergoes a significant tumble at $\tilde{x} = 0.2$, jumping above and to the left of the SwIM [Fig. 4(b)], with a corresponding change in direction in the $\tilde{x}\tilde{y}$ plane [Fig. 4(c)].

Despite the dramatic fluctuations in their orientations, the tumbling bacteria's $\tilde{x}\tilde{y}$ trajectories respect the vertical lines $\tilde{x} = \pm 1$ as one-way barriers, as predicted. Any RE swimmer must have entered with $\tilde{x} > -1$ [Fig. 4(d)], and any swimmer that enters with $\tilde{x} < -1$ must move leftward, away from the SwIM edge [Fig. 4(e)]. Furthermore, though the trajectories in Fig. 4(d) cross the horizontal passive manifold, they do not cross the lower red line at $\tilde{y} = -1$, respecting its outward-blocking nature.

In arbitrary flows, SwIM edges may not act as barriers for tumbling bacteria because they do not satisfy Eq. (3) in general. However, BIMs—which were introduced as one-way barriers to *front* propagation—always satisfy Eq. (3). In 2D time-independent flows, BIMs are the one-dimensional SwIMs for the $\alpha = -1$ case of Eq. (1) [i.e., $\alpha = -1$ trajectories $\mathbf{q}(t)$ that are asymptotic to SFPs], which satisfy the condition $-\mathbf{u}(\mathbf{r}(t)) \cdot \hat{\mathbf{n}}(t)/v_0 = 1$ [21,27,36]. Therefore, we now recognize BIMs as one-way barriers for all swimmers of a fixed swimming speed v_0, including those exhibiting rotational diffusion, tumbling, or other reorientation mechanisms. In particular, BIMs are

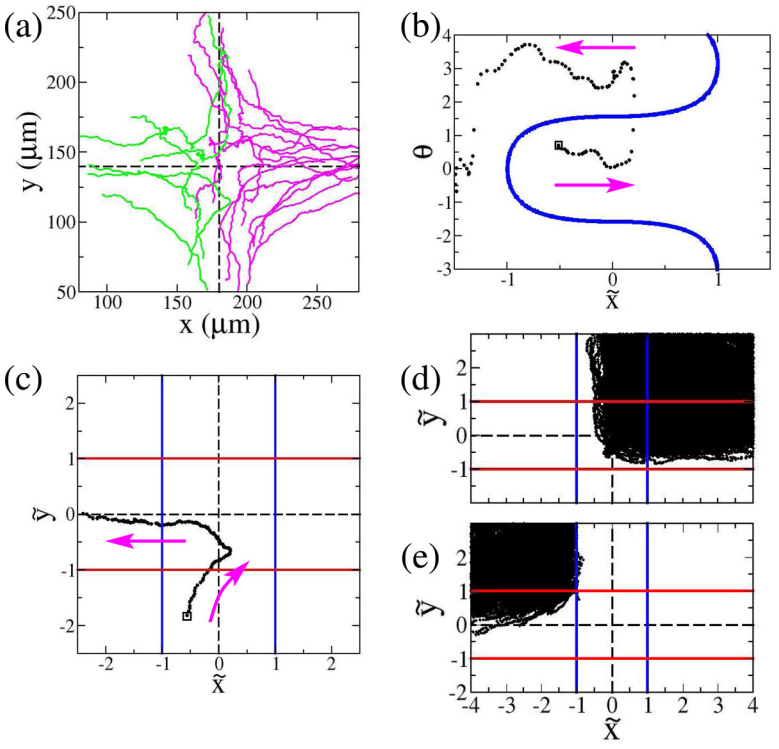

FIG. 4. (a) Selected trajectories of run-and-tumble *B. subtilis*; $A = 0.44\ \mathrm{s}^{-1}$. Passive manifolds are shown by dashed lines. (b) $\tilde{x}\theta$ plot and (c) $\tilde{x}\tilde{y}$ trajectory for a single bacterium with well-defined tumbling events. (d), (e) Scaled and rectified trajectories for tumbling bacteria, as in Figs. 2(d) and 2(e).

independent of the strength of the rotational noise, i.e., the swimmer's rotational Péclet number (Pe). Their structure is completely determined by the flow geometry, flow strength, and swimming speed. The robust bounding behavior occurs in our experiments because the SwIM edges coincide with the BIMs for linear hyperbolic flows, which are always the colored vertical and horizontal lines plotted in Fig. 1(b) at a distance v_0/A from the passive saddle point. In general nonlinear flows, on the other hand, SwIM edges and BIMs depart from each other. Thus, the SwIM edges are the more relevant barriers for perfect smooth swimmers, whereas the BIMs are more relevant for noisy swimmers, as we illustrate with the following example.

We consider the swimmer dynamics, Eq. (1), in the vortex-lattice flow [14,15,32,38] $\mathbf{u} = (\sin(2\pi\tilde{x})\cos(2\pi\tilde{y}), -\cos(2\pi\tilde{x})\sin(2\pi\tilde{y}))$, where we use nondimensional coordinates $\tilde{\mathbf{r}} = \mathbf{r}/L$ and $\tilde{t} = tU/L$ for a flow with maximum speed U and length scale L. Near $\mathbf{r} = 0$, the flow is approximately the linear hyperbolic flow, with $A = 2\pi$. Thus, the origin is surrounded by SFPs [Fig. 5(a)] analogous to those of Eq. (2) [32].

In analogy with the preceding microfluidic experiments that identified the positions of RE trajectories, we perform the following numerical experiment. We integrate the initial conditions of swimmers selected at random inside a single vortex cell but outside the gray square shown in Fig. 5(a). We then plot only those initial positions for which the swimmer trajectory enters the gray square at the upper edge $\tilde{y} = 0.25$ and subsequently exits through the right edge at $\tilde{x} = 0$ (see [36] for animations). These trajectories are analogous to the RE trajectories in the experimental hyperbolic flow. Figure 5(a) shows the result of the calculation for perfect smooth swimmers, along with the SwIM edge for the 2D stable SwIM of the vortex flow (solid curve) and the corresponding BIM (dotted curve). Clearly, these initial conditions are bounded by the SwIM edge,

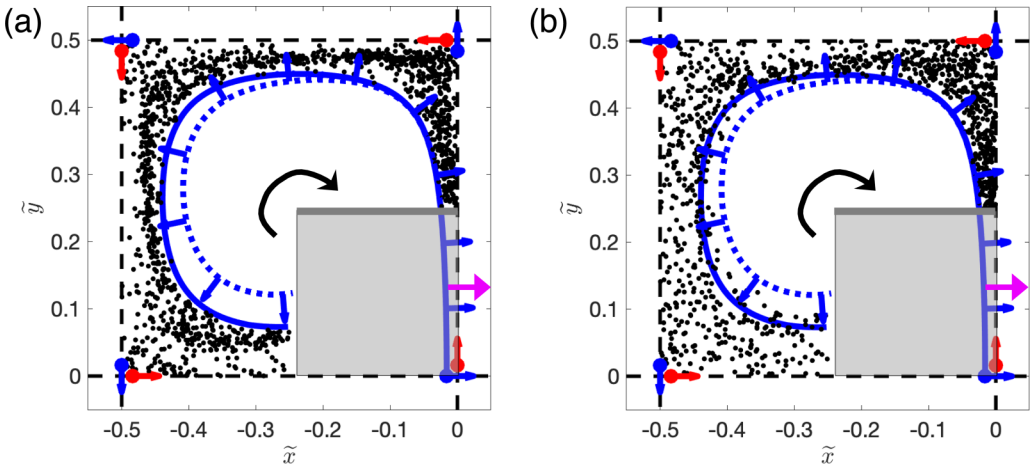

FIG. 5. Bounding properties of SwIM edges and BIMs in a vortex flow; $v_0/U = 0.1$, $\alpha = 1$. (a) Initial positions (black dots) of smooth swimmers that enter the gray square from the upper side and exit it on the right side (magenta arrow). The stable SwIM edge and stable BIM of the lower-right SFP are shown as solid blue and dotted blue curves, respectively. (b) Same as (a), for swimmers with rotational diffusivity D_r; $D_r L/U = 0.86$.

showing that the SwIM edge again bounds those trajectories that exit right, even in a nonlinear flow. We repeat the calculation with a moderate-intensity white-noise term added to $\dot{\theta}$ in Eq. (1) to simulate rotational diffusion for realistic smooth-swimming bacteria [34]. The resulting set of initial conditions [Fig. 5(b)] breaches the SwIM edge, but it remains bounded by the BIM, consistent with the absolute one-way barrier property of BIMs for all swimmers, regardless of their reorientation mechanism or Pe.

In summary, we have shown theoretically and experimentally that the trajectories of self-propelled particles in externally driven fluid flows are constrained by the presence of one-way barriers, i.e., SwIM edges and BIMs. Despite the simplicity of our model, we are able to fully explain certain properties of the trajectories of swimming bacteria in an externally driven microfluidic flow. Our SwIM framework provides a foundation for understanding the critical barrier structures that dominate the mixing of a wide range of self-propelled tracers in laminar flows. For example, BIMs must also block gyrotactic [39,40] and chemotactic swimmers, since these barriers are independent of biases in the swimming direction. We further expect that the SwIM approach can be generalized to more complicated, time-periodic, time-aperiodic, and weakly turbulent flows. It remains an open question how our approach may apply to the trajectories of self-propelled agents in active matter systems featuring self-driven flows, such as individual bacteria within a swarm [41] or motile defects in active nematics [42–44].

We thank Nico Waisbord and Jeff Guasto for providing the smooth-swimmer strain used in these experiments, Jack Raup and Joe Tolman for assistance with milling, Matt Heinzelmann for assistance with the incubation techniques, and Brandon Vogel for guidance on PDMS techniques. These studies were supported by the National Science Foundation under Grants No. DMR-1806355 and No. CMMI-1825379.

[1] J. Ottino, Mixing, chaotic advection, and turbulence, Annu. Rev. Fluid Mech. **22**, 207 (1990).
[2] H. Aref, J. R. Blake, M. Budišić, S. S. S. Cardoso, J. H. E. Cartwright, H. J. H. Clercx, K. El Omari, U. Feudel, R. Golestanian, E. Gouillart, G. J. F. van Heijst, T. S. Krasnopolskaya, Y. Le Guer, R. S. MacKay,

V. V. Meleshko, G. Metcalfe, I. Mezić, A. P. S. de Moura, O. Piro, M. F. M. Speetjens, R. Sturman, J.-L. Thiffeault, and I. Tuval, Frontiers of chaotic advection, Rev. Mod. Phys. **89**, 025007 (2017).

[3] R. S. MacKay, J. D. Meiss, and I. C. Percival, Transport in Hamiltonian systems, Phys. D (Amsterdam) **13**, 55 (1984).

[4] V. Rom-Kedar, A. Leonard, and S. Wiggins, An analytical study of transport, mixing and chaos in an unsteady vortical flow, J. Fluid Mech. **214**, 347 (1990).

[5] J. D. Meiss, Thirty years of turnstiles and transport, Chaos **25**, 097602 (2015).

[6] G. A. Voth, G. Haller, and J. P. Gollub, Experimental Measurements of Stretching Fields in Fluid Mixing, Phys. Rev. Lett. **88**, 254501 (2002).

[7] S. C. Shadden, F. Lekien, and J. E. Marsden, Definition and properties of Lagrangian coherent structures from finite-time Lyapunov exponents in two-dimensional aperiodic flows, Phys. D (Amsterdam) **212**, 271 (2005).

[8] C. Coulliette, F. Lekien, J. D. Paduan, G. Haller, and J. E. Marsden, Optimal pollution mitigation in Monterey Bay based on coastal radar data and nonlinear dynamics, Environ. Sci. Technol. **41**, 6562 (2007).

[9] M. Mathur, G. Haller, T. Peacock, J. E. Ruppert-Felsot, and H. L. Swinney, Uncovering the Lagrangian Skeleton of Turbulence, Phys. Rev. Lett. **98**, 144502 (2007).

[10] G. Haller, Lagrangian coherent structures, Annu. Rev. Fluid Mech. **47**, 137 (2015).

[11] M. Cencini, A. Torcini, D. Vergni, and A. Vulpiani, Thin front propagation in steady and unsteady cellular flows, Phys. Fluids **15**, 679 (2003).

[12] S. Saha, S. Atis, D. Salin, and L. Talon, Phase diagram of sustained wave fronts opposing the flow in disordered porous media, EPL **101**, 38003 (2013).

[13] B. Rhoads, I. Mezić, and A. C. Poje, Minimum time heading control of underpowered vehicles in time-varying ocean currents, Ocean Eng. **66**, 12 (2013).

[14] C. Torney and Z. Neufeld, Transport and Aggregation of Self-Propelled Particles in Fluid Flows, Phys. Rev. Lett. **99**, 078101 (2007).

[15] N. Khurana, J. Blawzdziewicz, and N. T. Ouellette, Reduced Transport of Swimming Particles in Chaotic Flow Due to Hydrodynamic Trapping, Phys. Rev. Lett. **106**, 198104 (2011).

[16] S. J. Ebbens and J. R. Howse, In pursuit of propulsion at the nanoscale, Soft Matter **6**, 726 (2010).

[17] J. Katuri, W. E. Uspal, J. Simmchen, A. Miguel-López, and S. Sánchez, Cross-stream migration of active particles, Sci. Adv. **4**, eaao1755 (2018).

[18] H. Wioland, F. G. Woodhouse, J. Dunkel, J. O. Kessler, and R. E. Goldstein, Confinement Stabilizes a Bacterial Suspension into a Spiral Vortex, Phys. Rev. Lett. **110**, 268102 (2013).

[19] R. Rusconi, J. S. Guasto, and R. Stocker, Bacterial transport suppressed by fluid shear, Nat. Phys. **10**, 212 (2014).

[20] J. Mahoney, D. Bargteil, M. Kingsbury, K. Mitchell, and T. Solomon, Invariant barriers to reactive front propagation in fluid flows, EPL **98**, 44005 (2012).

[21] K. A. Mitchell and J. R. Mahoney, Invariant manifolds and the geometry of front propagation in fluid flows, Chaos **22**, 037104 (2012).

[22] J. R. Mahoney and K. A. Mitchell, A turnstile mechanism for fronts propagating in fluid flows, Chaos **23**, 043106 (2013).

[23] J. R. Mahoney and K. A. Mitchell, Finite-time barriers to front propagation in two-dimensional fluid flows, Chaos **25**, 087404 (2015).

[24] R. A. Locke, J. R. Mahoney, and K. A. Mitchell, Mode-locking in advection-reaction-diffusion systems: An invariant manifold perspective, Chaos **28**, 013129 (2018).

[25] D. Bargteil and T. Solomon, Barriers to front propagation in ordered and disordered vortex flows, Chaos **22**, 037103 (2012).

[26] P. W. Megson, M. L. Najarian, K. E. Lilienthal, and T. H. Solomon, Pinning of reaction fronts by burning invariant manifolds in extended flows, Phys. Fluids **27**, 023601 (2015).

[27] J. R. Mahoney, J. Li, C. Boyer, T. Solomon, and K. A. Mitchell, Frozen reaction fronts in steady flows: A burning-invariant-manifold perspective, Phys. Rev. E **92**, 063005 (2015).

[28] M. Doan, J. J. Simons, K. Lilienthal, T. Solomon, and K. A. Mitchell, Barriers to front propagation in laminar, three-dimensional fluid flows, Phys. Rev. E **97**, 033111 (2018).
[29] A. Zöttl and H. Stark, Nonlinear Dynamics of a Microswimmer in Poiseuille Flow, Phys. Rev. Lett. **108**, 218104 (2012).
[30] J. A. Arguedas-Leiva and M. Wilczek, Microswimmers in an axisymmetric vortex flow, New J. Phys. **22**, 053051 (2020).
[31] S. Gu, T. Qian, H. Zhang, and X. Zhou, Stochastic dynamics of an active particle escaping from a potential well, Chaos **30**, 053133 (2020).
[32] S. A. Berman and K. A. Mitchell, Trapping of swimmers in a vortex lattice, Chaos **30**, 063121 (2020).
[33] G. Junot, N. Figueroa-Morales, T. Darnige, A. Lindner, R. Soto, H. Auradou, and E. Clément, Swimming bacteria in Poiseuille flow: The quest for active Bretherton-Jeffery trajectories, EPL **126**, 44003 (2019).
[34] J. T. Locsei and T. J. Pedley, Run and tumble chemotaxis in a shear flow: The effect of temporal comparisons, persistence, rotational diffusion, and cell shape, Bull. Math. Biol. **71**, 1089 (2009).
[35] Y. Hyon, Marcos, T. R. Powers, R. Stocker, and H. C. Fu, The wiggling trajectories of bacteria, J. Fluid Mech. **705**, 58 (2012).
[36] See Supplemental Material at http://link.aps.org/supplemental/10.1103/PhysRevFluids.6.L012501 for details on our experimental methods and data analysis, trajectories of nonswimming bacteria in the hyperbolic flow, a SwIM analysis of swimming bacteria trajectories at a lower flow rate, background information on BIMs, and details and animations of the vortex flow simulations, which includes Refs. [45] and [46].
[37] D. B. Kearns and R. Losick, Cell population heterogeneity during growth of Bacillus subtilis, Genes Dev. **19**, 3083 (2005).
[38] G. Ariel, A. Be'er, and A. Reynolds, Chaotic Model for Lévy walks in Swarming Bacteria, Phys. Rev. Lett. **118**, 228102 (2017).
[39] J. S. Guasto, R. Rusconi, and R. Stocker, Fluid mechanics of planktonic microorganisms, Annu. Rev. Fluid Mech. **44**, 373 (2012).
[40] M. Cencini, G. Boffetta, M. Borgnino, and F. De Lillo, Gyrotactic phytoplankton in laminar and turbulent flows: A dynamical systems approach, Eur. Phys. J. E **42**, 31 (2019).
[41] G. Ariel, A. Rabani, S. Benisty, J. D. Partridge, R. M. Harshey, and A. Be'Er, Swarming bacteria migrate by Lévy walk, Nat. Commun. **6**, 8396 (2015).
[42] T. Sanchez, D. T. Chen, S. J. Decamp, M. Heymann, and Z. Dogic, Spontaneous motion in hierarchically assembled active matter, Nature **491**, 431 (2012).
[43] S. Shankar, S. Ramaswamy, M. C. Marchetti, and M. J. Bowick, Defect Unbinding in Active Nematics, Phys. Rev. Lett. **121**, 108002 (2018).
[44] A. J. Tan, E. Roberts, S. A. Smith, U. A. Olvera, J. Arteaga, S. Fortini, K. A. Mitchell, and L. S. Hirst, Topological chaos in active nematics, Nat. Phys. **15**, 1033 (2019).
[45] J. C. Crocker and D. G. Grier, Methods of digital video microscopy for colloidal studies, J. Colloid Interface Sci. **179**, 298 (1996).
[46] M. T. Barry, R. Rusconi, J. S. Guasto, and R. Stocker, Shear-induced orientational dynamics and spatial heterogeneity in suspensions of motile phytoplankton, J. R. Soc. Interface **12**, 20150791 (2015).